

# A generalized theory of viscous and inviscid flutter

BY SHREYAS MANDRE AND L. MAHADEVAN\*

*School of Engineering and Applied Sciences, Harvard University, Pierce Hall,  
29 Oxford Street, Cambridge, MA 02138, USA*

We present a unified theory of flutter in inviscid and viscous flows interacting with flexible structures based on the phenomenon of 1:1 resonance. We show this by treating four extreme cases corresponding to viscous and inviscid flows in confined and unconfined flows. To see the common mechanism clearly, we consider the limit when the frequencies of the first few elastic modes are closely clustered and small relative to the convective fluid time scale. This separation of time scales slaves the hydrodynamic force to the instantaneous elastic displacement and allows us to calculate explicitly the dependence of the critical flow speed for flutter on the various problem parameters. We show that the origin of the instability lies in the coincidence of the real frequencies of the first two modes at a critical flow speed beyond which the frequencies become complex, thus making the system unstable to oscillations. This critical flow speed depends on the difference between the frequencies of the first few modes and the nature of the hydrodynamic coupling between them. Our generalized framework applies to a range of elasto-hydrodynamic systems and further extends the Benjamin–Landahl classification of fluid–elastic instabilities.

**Keywords:** fluid–structure interaction; flutter; 1:1 resonance

## 1. Introduction

Steadily forced flows interacting with elastic structures can spontaneously induce time-periodic oscillations. A commonly observed instance of such oscillations is evident in the fluttering of a flag (Zhang *et al.* 2000; Watanabe *et al.* 2002*b*). The phenomenon is not only limited to flags but manifests itself in a variety of systems such as the aeroelasticity of wings (Bisplinghoff *et al.* 1955; Bisplinghoff & Ashley 1962; Fung 2002; Dowell 2004), water- or wind-loaded buildings and structures (Billah & Scanlan 1991; Miyata 2003; Lemaitre & de Langre Hémon 2007), water hoses (Paidoussis 1998), thin-film coating and paper production processes (Chang & Moretti 2002; Watanabe *et al.* 2002*a,b*), physiology of blood and air flow (Korotkoff 1905; Bertram & Pedley 1982; Titze 1988; Pedley 1990; Huang 1998; Grotberg & Jensen 2004), musical instruments (Fletcher 1993; Tarnopolsky *et al.* 2000) and geophysical systems (Chouet 1985; Julian 1994; Balmforth *et al.* 2005; Müller *et al.* 2005; Rust *et al.* 2007). The origin of such flutter is usually attributed to an oscillatory instability of a steady state when the fluid flow exceeds

\*Author for correspondence (lm@deas.harvard.edu).

a threshold, and is referred to as an instance of a Poincaré–Andronov–Hopf (PAH) bifurcation. Moreover, fluid inertia is the dominant destabilizing mechanism for most of these cases. Here, we use a systematic reduction of the continuum equations and show that the common underlying mechanism for flutter in a broad class of examples including the systems listed is not the usual PAH scenario but instead involves the concept of a 1:1 resonance, as used to explain vortex-induced vibrations (Paidoussis 1998) and the onset of flag flutter (Argentina & Mahadevan 2005), for example. This systematic reduction, when performed for viscous flows, reveals new instabilities, where viscosity and not inertia is the dominant destabilizing agency.

To see this, we first review the 1:1 resonance mechanism, so called because it involves a coincidence of two frequencies in a dynamical system, which was first described by Kelvin & Tait (1912). In its simplest form, it requires the consideration of two asymmetrically coupled undamped linear oscillators whose amplitudes  $A$  and  $B$  satisfy

$$\frac{d^2}{dt^2} \begin{bmatrix} A \\ B \end{bmatrix} = \begin{bmatrix} -\Omega_1^2 & 0 \\ 0 & -\Omega_2^2 \end{bmatrix} \begin{bmatrix} A \\ B \end{bmatrix} + F \begin{bmatrix} 0 & 1 \\ -1 & 0 \end{bmatrix} \begin{bmatrix} A \\ B \end{bmatrix}. \quad (1.1)$$

The coupling is assumed to have gyroscopic form, i.e. it is skew symmetric, with the coupling constant  $F$ , although this condition of skew symmetry is not necessary, and indeed is not always respected in the systems we consider. When  $F=0$ , the uncoupled system has two distinct natural frequencies  $\Omega_1$  and  $\Omega_2$ , respectively. When  $F \neq 0$ , solving the characteristic equation associated with equation (1.1) yields the modified frequencies of the system as

$$\tilde{\Omega}_{1,2}^2 = \frac{\Omega_1^2 + \Omega_2^2 \pm \sqrt{(\Omega_1^2 - \Omega_2^2)^2 - 4F^2}}{2}. \quad (1.2)$$

We see that when the discriminant in equation (1.2) becomes negative,  $\tilde{\Omega}_{1,2}$  takes on complex conjugate values, so that the frequency acquires an imaginary part and the system exhibits exponential growth.

We will show that in hydroelastic or aeroelastic systems, the normal modes of the elastic body constitute the oscillators while the fluid forcing on the elastic structure is proportional to the coupling constant  $F$ . Then, as can be inferred from equation (1.2), the critical  $F = F_c = |\Omega_1^2 - \Omega_2^2|/2$  is proportional to the difference of the natural frequencies of the two modes. Throughout, we will limit our analysis to the linearized problem where we can see the mechanism of onset of the instability clearly; although nonlinearity eventually limits this growth, it will not concern us in this paper.

One inspiration for this work comes from Rocard (1957), who first presented the mechanism of 1:1 resonance in the context of wing and bridge flutter and derived a system of equations similar to equation (1.1). We delineate the three assumptions that are inherent in his derivation, as we will use these as well:

- (i) The fluid dynamic forces are weak compared with both the elastic forces and structural inertia, so that the dynamics of the system are dominated by the normal mode oscillations of the elastic structure. This allows us to then compute the fluid forcing perturbatively.

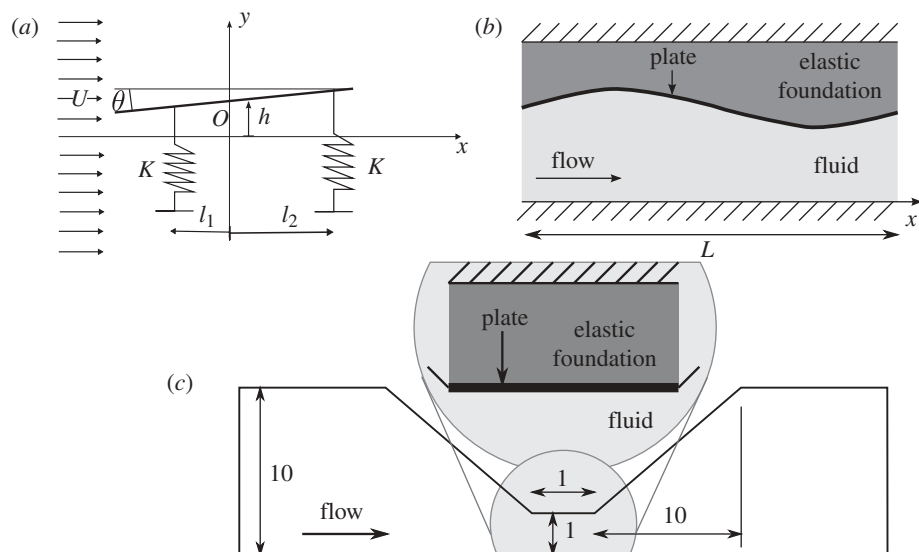


Figure 1. Schematic of the representative systems modelled for flow in external and confined geometries. (a) the model system for fluid flow in an unconfined geometry. The system consists of a rigid flat plate supported by two springs, as a result of which the structure has two degrees of freedom. The far-field fluid flow is parallel to the plate and could be viscous (small Reynolds number) or inviscid (large Reynolds number). (b) schematic model for flow in a confined geometry. The system consists of a channel with a flexible wall. The wall is supported by a distributed set of springs and can have a bending stiffness and a tension. If the flow through the channel is viscous (low Reynolds number) then the channel connects two reservoirs at constant pressure. (This case is treated analytically.) For inviscid flow (high Reynolds number), a completely analytical treatment is not possible and we consider a numerical solution for the fluid flow. For this case, we consider a converging–diverging channel as shown in (c). (c) the inset shows a magnified view of the flexible part of the channel wall.

- (ii) The natural frequencies of the first few modes of oscillations are closely clustered. This allows even a relatively weak fluid forcing to couple the dominant modes and thus provides the conditions for the onset of 1 : 1 resonance.
- (iii) The hydrodynamic time scale is much smaller than the natural time scale of oscillation of the elastic system. This means that the hydrodynamic force is enslaved to the instantaneous shape of the structure and is independent of the rate of change of this shape to leading order.

We show that these assumptions apply to a range of systems and allow us to quantify the conditions for the spontaneous appearance of oscillations in a variety of situations involving viscous and inviscid flows in confined and unconfined geometries. To probe the geometric and hydrodynamic extremes of aeroelastic and hydroelastic flutter, we consider four different cases: inviscid flutter in unconfined and confined geometries and viscous flutter in unconfined and confined geometries, shown schematically in figure 1. In §2, we analyse inviscid and viscous flows in unconfined geometries, while in §3, we analyse inviscid and viscous flows in confined geometries. Finally, in §4, we conclude with a discussion that places our work in the broader context of fluid elastic interaction.

## 2. Flutter in unconfined geometries

On large scales, flutter in unconfined flows arises in such examples as the aeroelasticity of wings and bridges, when subject to a fluid loading. On small scales, examples include the flutter of elastic plates and membranes in very viscous flows that arise in microfluidic applications, for example. These elastic bodies are typically slender, i.e. their length is typically much larger than their widths, which in turn is much larger than their thickness. As a result, to leading order, a long wavelength description of their behaviour implies that their deformation is dominated by bending and twisting, which give rise to a translation and rotation of individual cross sections. If these deformations are sufficiently small, then a physically and geometrically linear theory suffices to describe the elastic response, which amounts to a restoring force and torque for the translational and rotational degrees of freedom.

As a representative example of this simple model, we consider a rigid object (either a plate or a rod) supported by two springs as shown in figure 1, with two degrees of freedom, vertical translation and rotation about the centre. For aircraft wings and bridges, the translational mode is analogous to bending of the wing along the spanwise direction, moving a cross section of the wing up and down, while the rotational mode represents wing twist. For a suspension bridge, the tension in the suspending cables is also a contributor along with bending and torsion, as elucidated by Rocard (1957), among others. In the inviscid flow case, we let the object be a rigid flat plate. For external viscous flow, we replace the aerofoil with a thin rod aligned in the direction of flow. The undisturbed position of the centre of the object is taken as the origin  $O$  with the plane of the plate (or the axis of the rod) aligned with the  $x$ -axis. Two springs of stiffness  $K$  located asymmetrically at a distance  $l_1$  and  $l_2$  from the plate centre provide support. This asymmetry causes the centre of lift to differ from the centre of rotation for the plate; this will eventually be linked to the possibility of flutter. The dynamic variables  $h(t)$  and  $\theta(t)$  characterize the instantaneous configuration of the plate, so that the location of the plate is given in terms of these variables by

$$y = h(t) + \theta(t)x \quad (2.1)$$

and the governing equations for the dynamics of the structure are

$$Mh_{tt} = -2Kh + 2K\theta\Delta l + F_h \quad (2.2)$$

and

$$M\kappa^2\theta_{tt} = 2K\Delta lh - 2K\ell^2\theta + T_h, \quad (2.3)$$

where  $(\cdot)_t = d/dt$ ,  $M$  is the mass per unit length of the plate (or the rod),  $\kappa$  is its radius of gyration,  $2\Delta l = l_1 - l_2$ ,  $2\ell^2 = l_1^2 + l_2^2$ ,  $F_h$  is the hydrodynamic lift force and  $T_h$  is the hydrodynamic torque. The natural frequencies of oscillations for this system in the absence of any fluid coupling are given by

$$\Omega_{1,2}^2 = \frac{2K}{M} \left( \frac{\kappa^2 + \ell^2}{2\kappa^2} \pm \sqrt{\frac{(\kappa^2 - \ell^2)^2}{4\kappa^4} + \frac{\Delta l^2}{\kappa^2}} \right). \quad (2.4)$$

To understand how fluid loading changes these frequencies, we now consider the case of inviscid and viscous flows separately.

(a) *Inviscid case*

When the Reynolds number based on the length  $L$  of the elastic plate  $Re = UL/\nu \gg 1$ , where  $U$  is the free stream velocity, and  $\nu = \mu/\rho$  is the kinematic viscosity, inertial effects dominate viscous forces, so that we may approximate the effects of the flow using potential flow theory, with a velocity potential  $\phi$  characterizing the velocity field  $\mathbf{u} = \nabla\phi$ . Furthermore, the pressure in the fluid is then given by the unsteady Bernoulli equation  $p + \rho\phi_t + \rho(u^2 + v^2 + w^2)/2 = \text{constant}$ , which relation allows us to calculate the forces on the elastically supported plate, modelled here as a thin aerofoil.

When the far-field flow is oriented with the stationary orientation of the plate, both  $h = \theta = 0$ , and in the absence of vorticity, the hydrodynamic force is also zero by symmetry. Assuming that the aerofoil oscillates with a small amplitude and a frequency  $\Omega$ , the hydrodynamic force can be computed by determining the perturbed velocity components  $(u, v)$  in terms of a disturbance potential  $\phi$ , which satisfies

$$(u, v) = \nabla\phi, \quad \nabla^2\phi = 0 \quad \text{with } h_t + Uh_x = \phi_y \quad \text{on the aerofoil,} \quad (2.5)$$

subject to the Kutta condition that  $\nabla\phi$  is finite at the trailing edge (Batchelor 1967). Then the linearized Bernoulli equation yields the disturbance pressure  $p = -\rho(\phi_t + U\phi_x)$  due to the motion and orientation of the plate. To understand the contributions to the pressure from the flow, we first decompose the solution to equation (2.5) by writing  $\phi = \phi_1 + \phi_2$ , where  $\nabla^2\phi_1 = \nabla^2\phi_2 = 0$ ,  $\phi_{1y} = Uh_x$  arising from the instantaneous conformation and  $\phi_{2y} = h_t$  arising from the instantaneous rate of change of the plate. Then we write the pressure difference between the two sides of the plate as  $p = p_1 + p_2 + p_3$ , where  $p_1 = -\rho U\phi_{1x}$ ,  $p_2 = -\rho(\phi_{1t} + U\phi_{2x})$  and  $p_3 = -\rho\phi_{2t}$ . Since  $\partial_t \propto \Omega$  and  $U\partial_x \propto U/L$ ,  $p_1/p_2 \sim p_2/p_3 \sim \Omega L/U = \epsilon$ .

We now consider the three assumptions outlined in the introduction. Assumption (i) implies that  $F_h \ll Kh$  and  $T_h \ll Kh\ell$ . Assumption (ii) implies that  $\Omega_1 \approx \Omega_2$ , which in turn implies that  $\ell \approx \kappa$  and  $\Delta l \ll \kappa$ . We restrict ourselves to  $\ell = \kappa$ . Assumption (iii) implies that the hydrodynamic time scale is much smaller than the elastic time scale, i.e.  $\Omega L \ll U$  so that  $p_1 \ll p_2 \ll p_3$ . Quantitatively, assumptions (i) and (iii) can be summarized as  $M\Omega^2 = 2K \gg \rho U^2/L \gg \rho\Omega U \gg \rho\Omega^2 L$ .

Translational invariance implies that the quasi-steady lift force or the torque on the aerofoil cannot depend on  $h$ . Thus, the hydrodynamic coupling between  $h$  and  $\theta$  for an arbitrary aerofoil in a flow satisfying the quasi-steady linearized Navier–Stokes equations will be asymmetric. For analytical simplicity we restrict ourselves to thin aerofoil theory which gives (Theodorsen 1935; Argentina & Mahadevan 2005)

$$\Delta p(x, t) \approx -\rho UC(\epsilon)f\left(\frac{x}{L}\right)(h_t + x\theta_t + U\theta), \quad (2.6)$$

where  $\Delta p$  is the difference in pressure on the two sides of the plate and the Theodorsen (1935) function  $C(s)$ , and  $f(s)$  are given by

$$C(s) = \frac{H_1^{(2)}(s)}{H_1^{(2)}(s) + iH_0^{(2)}(s)} \quad \text{and} \quad f(s) = 2\sqrt{\frac{1-2s}{1+2s}}, \quad (2.7)$$

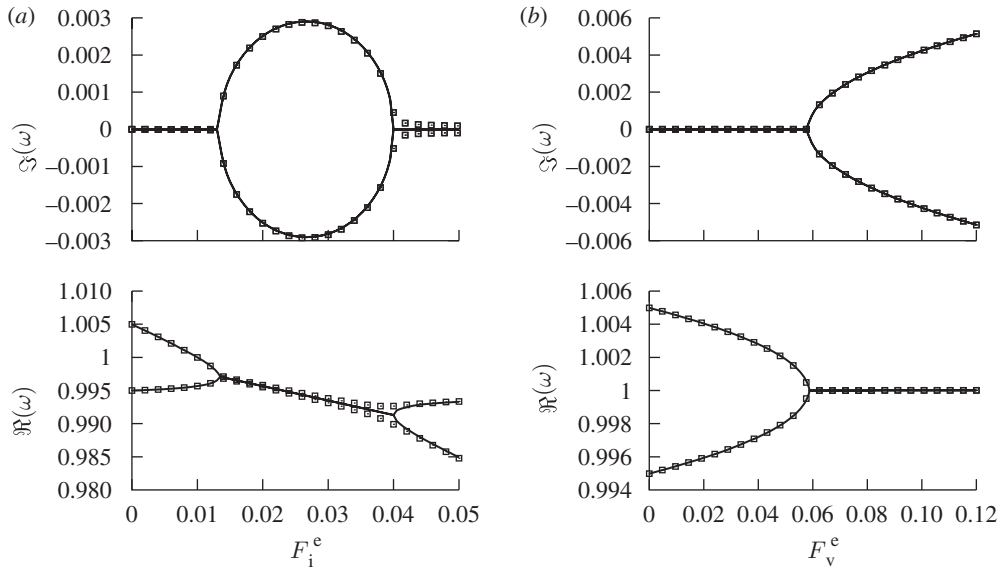


Figure 2. The real and imaginary parts of the natural frequency of oscillations for unconfined flows external to the elastic structure (see schematic in figure 1). A negative imaginary part implies growth of oscillatory perturbation leading to spontaneously generated flutter. The spectrum for (a) the inviscid flow approximation following equation (2.9) and (b) the spectrum for the viscous approximation following equation (2.14). The parameters used are  $\Delta l = 0.01$ ,  $L = \sqrt{12}$ ,  $\epsilon = 0$  (solid line) and  $\epsilon = 10^{-4}$  (squares). The aspect ratio  $\phi$  of the rod was set to 10 for the solution of equation (2.14).

$H_j^{(2)}$  being the Hankel functions of order  $j$ . Then, we may evaluate the hydrodynamic force and torque

$$F_h = \int_{-L/2}^{L/2} \Delta p \, dx \quad \text{and} \quad T_h = \int_{-L/2}^{L/2} x \, \Delta p \, dx. \quad (2.8)$$

Using the scaling  $(h, \Delta l, L) \rightarrow \kappa(h, \Delta l, L)$ ,  $t \rightarrow t/\Omega$  in equations (2.2) and (2.3), letting  $F_i^e = \pi \rho U^2 L / K \kappa$  (where the subscript  $i$  stands for inviscid and the superscript  $e$  stands for external flow) and performing the integrals involving  $p$  in equation (2.8) to  $O(\epsilon)$  yield

$$\begin{aligned} \frac{d^2}{dt^2} \begin{bmatrix} h \\ \theta \end{bmatrix} &= \begin{bmatrix} -1 & \Delta l \\ \Delta l & -1 \end{bmatrix} \begin{bmatrix} h \\ \theta \end{bmatrix} - F_i^e \left(1 + \frac{\epsilon \pi}{2}\right) \begin{bmatrix} 0 & 1 \\ 0 & -\frac{1}{L} \end{bmatrix} \begin{bmatrix} h \\ \theta \end{bmatrix} \\ &\quad - \epsilon F_i^e \begin{bmatrix} 1 & \gamma + \ln \frac{\epsilon}{2} - \frac{1}{4} \\ -\frac{L}{4} & L \left(\frac{1}{8} - \gamma - \ln \frac{\epsilon}{2}\right) \end{bmatrix} \begin{bmatrix} h_t \\ \theta_t \end{bmatrix}, \end{aligned} \quad (2.9)$$

where  $\gamma$  is the Euler–Mascheroni constant.

These coupled linear second-order ordinary differential equations are similar to the canonical form (1.1) and can be solved by substituting  $(h, \theta) \propto e^{i\omega t}$  to yield an eigenvalue problem for  $\omega$ . In figure 2a, we plot the real and imaginary parts of

the frequency  $\omega$  using the parameter values  $L = \sqrt{12}$  and  $\Delta l = 0.01$ . For  $\epsilon = 0$  the spectrum is similar to that associated with equation (1.2), with the frequencies given by

$$\omega_{1,2}^2 = 1 + \frac{-F_i^e L \pm \sqrt{F_i^{e2} L^2 + 64\Delta l(\Delta l - F_i^e)}}{8}. \quad (2.10)$$

The frequencies split into complex conjugate pairs in an interval  $F_{i,c1}^e = \frac{4}{3}\Delta l < F_i^e < 4\Delta l = F_{i,c2}^e$  corresponding to the window of parameters where the system is susceptible to flutter. The presence of a finite window is associated with the fact that the hydrodynamic coupling is not skew symmetric, i.e. it is not of gyroscopic form. Since  $\Delta l$  measures the difference in the natural frequency of oscillations of the two modes, the critical values of  $F_i^e$  scale with this difference in frequency. When  $\epsilon > 0$ , although the frequencies are complex for all  $F_i^e$  due to the  $O(\epsilon)$  term in equation (2.9), they are well approximated by the case corresponding to  $\epsilon = 0$ . This unfolding of the 1:1 resonance mode can then lead to a scenario that is superficially similar to a PAH bifurcation, although both the underlying mechanisms and the mathematical description as encoded in the normal forms for the two scenarios are quite different.

(b) *Viscous case*

When the Reynolds number of the flow is small, inertia is overwhelmed by viscous forces. Then, we may use the Stokes approximation to approximate the flow around a body. Pressure gradients are balanced by viscous forces, so that  $\nabla p = \mu \nabla^2 u$ , while the condition of incompressibility reads  $\nabla \cdot u = 0$ . A general consequence of the linearity of Stokes equations is that in the absence of free boundaries, the lift force and the torque on a rigid body immersed in a fluid are proportional to the velocity of the body multiplied by a resistance matrix (Happel & Brenner 1983). Decomposing the viscous forces and torques into components because of the change in orientation of the rod, and the resistance to translation ( $h_t$ ) and rotation ( $\theta_t$ ) allows us to write

$$F_h = -\hat{\mathbf{y}} \cdot (\mu L \mathbf{Q}^T \cdot \mathbf{R}_U \cdot \mathbf{Q} \cdot (U \hat{\mathbf{x}} + h_t \hat{\mathbf{y}}) + \mu L^2 \mathbf{Q}^T \cdot \mathbf{C} \theta_t) \quad (2.11)$$

and

$$T_h = -\mu L^2 \mathbf{C} \cdot \mathbf{Q} \cdot (U \hat{\mathbf{x}} + h_t \hat{\mathbf{y}}) - \mu L^3 \mathbf{R}_\Omega \theta_t. \quad (2.12)$$

Here  $\mathbf{R}_U$  is the resistance matrix to translation,  $\mathbf{R}_\Omega$  is the resistance to rotation,  $\mathbf{C}$  is the coupling matrix and  $\mathbf{Q} = (\hat{\mathbf{x}}\hat{\mathbf{x}} + \hat{\mathbf{y}}\hat{\mathbf{y}}) \cos \theta + (\hat{\mathbf{x}}\hat{\mathbf{y}} - \hat{\mathbf{y}}\hat{\mathbf{x}}) \sin \theta$  is the two-dimensional rotation matrix corresponding to rotation by an angle  $\theta$ . The two resistance matrices  $\mathbf{R}_U$  and  $\mathbf{R}_\Omega$  and the coupling matrix  $\mathbf{C}$  depend only on the shape of the body but not on its size.

We now consider the three assumptions outlined in the introduction. Assumption (i) requires that  $F_h \ll Kh$  and  $T_h \ll Kh\ell$ . Since the hydrodynamic force scales like  $\mu UL$ , where  $\mu$  is the dynamic viscosity of the fluid, assumption (i) implies that  $\mu U \ll K$ , i.e. the elastic structure is stiff. Assumption (ii) implies that  $\Omega_1 \approx \Omega_2$ , which in turn implies that  $\ell \approx \kappa$  and  $\Delta l \ll \kappa$ . And once again from assumption (iii) we see that the forces and torques proportional to  $h_t$  and  $\theta_t$  are

a factor of  $\epsilon = \Omega L/U$  smaller than the corresponding terms proportional to  $h$  and  $\theta$ . While this argument is valid for an arbitrary body, we present the specific example of a slender rod as a representative case for which the resistance matrices only depend on the aspect ratio of the rod ( $\phi$ ) and are given by

$$\mathbf{R}_U = \frac{4\pi}{2 \ln 2\phi + 1} \hat{\mathbf{x}}\hat{\mathbf{x}} + \frac{8\pi}{2 \ln 2\phi - 1} \hat{\mathbf{y}}\hat{\mathbf{y}}, \quad \mathbf{C} = \mathbf{0} \quad \text{and} \quad \mathbf{R}_\Omega = \frac{\pi}{6 \ln 2\phi - 3}. \quad (2.13)$$

Substituting equations (2.11) and (2.12) in equations (2.2) and (2.3) and using the dimensionless variables  $(h, \Delta l) \rightarrow \kappa(h, \Delta l)$ ,  $t \rightarrow t/\Omega$  yield the dynamical system

$$\begin{aligned} \frac{d^2}{dt^2} \begin{bmatrix} h \\ \theta \end{bmatrix} &= \begin{bmatrix} -1 & \Delta l \\ \Delta l & -1 \end{bmatrix} \begin{bmatrix} h \\ \theta \end{bmatrix} - F_v^e g(\phi) \begin{bmatrix} 0 & 1 \\ 0 & 0 \end{bmatrix} \begin{bmatrix} h \\ \theta \end{bmatrix} \\ &- \epsilon F_v^e \begin{bmatrix} \frac{8}{2 \ln 2\phi + 1} & 0 \\ 0 & \frac{L^2}{6 \ln 2\phi - 3} \end{bmatrix} \begin{bmatrix} h_t \\ \theta_t \end{bmatrix}, \end{aligned} \quad (2.14)$$

where we introduce the dimensionless parameter  $F_v^e$  (subscript v for viscous and superscript e for external flow) and the function  $g(\phi)$  as

$$F_v^e = \frac{\pi \mu U}{K} \quad \text{and} \quad g(\phi) = \frac{4 \ln 2\phi - 6}{4(\ln 2\phi)^2 - 1}. \quad (2.15)$$

The origin of the lift that couples the rotation of the rod to a normal force comes from the fact that for an anisotropic body, the viscous resistance to motion is not necessarily in the direction of motion because the resistance matrix is itself anisotropic, i.e. the drag coefficients in different directions are different. The natural frequencies  $\omega$  of oscillation can be obtained by solving the characteristic equation associated with equation (2.14). This can be done analytically for  $\epsilon = 0$  to get

$$\omega_{1,2}^2 = 1 + \sqrt{\Delta l(\Delta l - F_v^e g(\phi))}. \quad (2.16)$$

The frequencies of the modes split into complex conjugate pairs when  $F_v^e g(\phi) > \Delta l$ , as shown in figure 2b. We see that the critical value of  $F_v^e$  is proportional to the difference in natural frequencies of the two modes just as in the inviscid case. For  $\epsilon > 0$ , the complex conjugate frequencies of equation (2.14) must be obtained numerically; however once again, for small  $\epsilon$  they are well approximated by the solutions corresponding to the  $\epsilon = 0$  case as seen in figure 2b.

### 3. Flutter in confined flows

Flutter in confined flows arises in a number of biological applications such as controlled vocal phonation, snoring and wheezing, as well as Korotkoff sounds in blood vessels, in engineering applications such as flutter in thin-film coating and paper production processes and in geological systems associated with subvolcanic tremors and the singing of glaciers. The main effect of confinement is the separation of scales in the hydrodynamic problem that leads to a qualitative difference in the flow profiles and the associated forces. A concrete realization

of this shown in figure 1 considers a channel of length  $L$  and width  $H$  with flexible walls. The wall is assumed to have an elastic plate as a skin, supported by a compressible elastic foundation. With biological applications to phonation in mind, we assume that the foundation thickness is much thinner than its longitudinal extent, and further, that the elastic plate is assumed to be even thinner than the foundation, but much stiffer.

Then we may write the governing equation for the displacement of the channel wall  $h(x, t)$  as

$$Mh_{tt} + \Sigma h_t = -K(h - H) + Th_{xx} - Bh_{xxxx} + p(x, t), \quad (3.1)$$

where  $M$  is the lumped linear density of the elastic composite,  $\Sigma$  is the damping constant,  $K$  is the equivalent spring stiffness originating from the deformation of the elastic foundation,  $T$  is the tension in the plate in the  $x$ -direction and  $B$  is its bending rigidity and  $p(x, t)$  denotes the fluid pressure in the channel. Using the scaling

$$t \longrightarrow t/\Omega, \quad x \longrightarrow Lx, \quad h \longrightarrow Hh \quad \text{and} \quad p \longrightarrow Pp, \quad (3.2)$$

where  $\Omega = \sqrt{K/M}$  and  $P$  depends on the fluid model then converts equation (3.1) to

$$h_{tt} + \sigma h_t = 1 - h + \frac{\tau}{\pi^2} h_{xx} - \frac{\beta}{\pi^4} h_{xxxx} + \frac{P}{KH} p, \quad (3.3)$$

where  $\sigma = \Sigma\Omega/K$  is the dimensionless damping constant,  $\tau = T\pi^2/KL^2$  the dimensionless tension and  $\beta = B\pi^4/KL^4$  the dimensionless bending stiffness. For this spatially extended elastic system, we need to specify some boundary conditions. While the procedure we use is applicable to any boundary conditions that render the problem self-adjoint in the absence of the fluid, we restrict ourselves here to  $h = h_{xx} = 0$  at  $x = 0, L$ . Then the natural modes of oscillations of the elastic wall are

$$h_n = \sin(n\pi x), \quad n = 1, 2, 3, \dots \quad (3.4)$$

Expanding the solution  $h$  as a time-dependent linear combination of these modes, we write

$$h = 1 + \sum_{n=1}^{\infty} A_n(t) h_n(x), \quad (3.5)$$

where  $A_n(t)$  denote the mode amplitude. Substituting this expansion in equation (3.1), multiplying by  $h_n(x)$  and integrating over the domain  $0 < x < L$ , i.e. projecting back on the mode shapes, we obtain a set of equations for the mode amplitudes

$$\frac{d^2 A_n}{dt^2} + \sigma \frac{dA_n}{dt} = - (1 + \tau n^2 + \beta n^4) A_n + \frac{2P}{KH} \int_0^1 p h_n dx. \quad (3.6)$$

To understand how fluid loading changes these frequencies via the hydrodynamic coupling induced by pressure, we now consider the case of inviscid and viscous flows separately.

(a) *Viscous flow*

For viscous flow through long narrow channels ( $H/L \ll 1$ ) and the Reynolds number based on the gap  $UH/\nu \ll 1$ , the dimensional form of  $x$ -momentum balance in the two-dimensional Navier–Stokes equations simplifies to the well-known lubrication approximation (Batchelor 1967)  $p_x = \mu u_{yy}$ ,  $p_y = 0$  coupled with the incompressibility condition  $u_x + v_y = 0$ . Integrating the two momentum balance equations with the no-slip boundary condition at  $y = 0$  and  $h$  yields the horizontal velocity  $u = -p_x y(h - y)/2\mu$ . Conservation of mass  $h_t + \int_0^h u \, dy = 0$  then yields an equation relating pressure and the motion of the boundary as

$$h_t = \frac{1}{12\mu} (h^3 p_x)_x. \quad (3.7)$$

We assume that the channel opens on both sides into infinite reservoirs, which maintains the fluid pressure constant, and results in a steady-state flux  $UH$ . Scaling  $h$ ,  $x$  and  $t$  according to equation (3.2) and choosing  $P = 12\mu UL/H^2$  simplifies equation (3.7) to

$$\epsilon h_t = (h^3 p_x)_x, \quad (3.8)$$

where  $\epsilon = \Omega L/U$  as before and the boundary conditions on  $p$  are  $p(x = 0) = 1$  and  $p(x = 1) = 0$ .

We now consider the three assumptions outlined in the introduction. Assumption (i) requires that the hydrodynamic pressure is small compared with the elastic forces, i.e.  $P \ll KH$ . As a result, the equilibrium shape of the membrane to leading order is  $h = 1 + O(P/KH)$  and the dominant dynamics are oscillations of each mode with its natural frequency  $\Omega_n^2 = 1 + \tau n^2 + \beta n^4$ . In particular, this now implies  $2P/\pi KH = 24\mu UL/\pi KH^3 \equiv F_v^c \ll 1$ , where the subscript  $v$  stands for viscous flow and the superscript  $c$  stands for confined flow. As a consequence, in steady state  $h = 1 + O(F_v^c)$  and  $p = 1 - x + O(F_v^c)$ . Assumption (ii) requires that the modes are clustered together. If  $\tau = \beta = 0$ , the system is infinitely degenerate with unit frequency, but when  $\tau, \beta \ll 1$  the non-dimensional frequencies of the first few modes are close to unity. Finally, assumption (iii) that the hydrodynamic time scale be smaller than the elastic time scale implies  $\epsilon \ll 1$ .

By substituting the modal expansion (3.5) in equation (3.8), with the assumption that the amplitudes  $A_n$ 's are small leads to an expression for the fluid pressure

$$p = 1 - x + \sum_{n=1}^{\infty} -\frac{\epsilon}{n^2 \pi^2} \frac{dA_n}{dt} \sin n\pi x + \frac{3A_n}{n\pi} [1 - \cos n\pi x - x(1 - \cos n\pi)] + O(F_v^c), \quad (3.9)$$

which is the dominant contribution to the response of the fluid flow to wall motion. Substituting equation (3.9) in equation (3.6) leads to the following linearized

system for the evolution of the modal amplitudes:

$$\begin{aligned} \frac{d^2 A_n}{dt^2} + \sigma \frac{dA_n}{dt} = & -(1 + \tau n^2 + \beta n^4) A_n + \frac{2F_v^c}{n\pi} - \frac{\epsilon F_v^c}{n^2 \pi^2} \frac{dA_n}{dt} \\ & - \frac{3F_v^c}{\pi} \sum_{m=1, m \neq n}^{\infty} A_m \frac{m}{n} \left( \frac{1 - (-1)^{m+n}}{n^2 - m^2} \right). \end{aligned} \quad (3.10)$$

Truncating this system by keeping just the first two modes yields

$$\begin{aligned} \frac{d^2}{dt^2} \begin{bmatrix} A_1 \\ A_2 \end{bmatrix} + \sigma \frac{d}{dt} \begin{bmatrix} A_1 \\ A_2 \end{bmatrix} = & \begin{bmatrix} -1 - \tau - \beta & 0 \\ 0 & -1 - 4\tau - 16\beta \end{bmatrix} \begin{bmatrix} A_1 \\ A_2 \end{bmatrix} + \frac{F_v^c}{\pi} \begin{bmatrix} 2 \\ 1 \end{bmatrix} \\ & - \frac{F_v^c}{2\pi} \begin{bmatrix} 0 & -4 \\ 1 & 0 \end{bmatrix} \begin{bmatrix} A_1 \\ A_2 \end{bmatrix} - \frac{\epsilon F_v^c}{4\pi^2} \begin{bmatrix} 4 & 0 \\ 0 & 1 \end{bmatrix} \begin{bmatrix} A_{1t} \\ A_{2t} \end{bmatrix}. \end{aligned} \quad (3.11)$$

Substituting  $A_1, A_2 \sim e^{i\omega t}$  in equation (3.11) yields a characteristic equation for the eigenvalues, which in general has complex solutions owing to the terms proportional to  $A_{nt}$  coming from the damping  $\sigma$  and the non-quasi-steadiness  $\epsilon$ . However, when  $\epsilon = 0$  and  $\sigma = 0$ , the coefficients in the characteristic polynomial are real and have as their solutions the natural frequencies

$$\omega_{1,2}^2 = 1 + \frac{1}{2} \left( 5\tau + 17\beta \pm \sqrt{(3\tau + 15\beta)^2 - \frac{4F_v^c{}^2}{\pi^2}} \right) \quad (3.12)$$

plotted in figure 3*b*. We see that the frequencies are real for  $F_v^c < \pi(3\tau + 15\beta)/2$  and split into complex conjugate pairs for  $F_v^c > \pi(3\tau + 15\beta)/2$ . As before the critical value of  $F_v^c \propto (3\tau + 15\beta)$ , i.e. it is proportional to the difference between the frequencies of the first two elastic modes. When  $\epsilon > 0$ , the results resemble those for which  $\epsilon = 0$  is the case as can be seen from figure 3. Indeed, equation (3.11) shows that the effect of a small  $\epsilon$  is equivalent to adding a small but mode-dependent amount of damping in the equation for the mode amplitude.

We also compare the frequencies obtained in equation (3.12) with the linear stability of the steady state of equations (3.3) and (3.8) without any further approximations. To do that, we define the steady state  $h(x, t) = H_0(x)$  and  $p(x, t) = P_0(x)$  by the solution of

$$\left. \begin{aligned} H_0^3 P_{0x} = 0, \quad 1 - H_0 + \frac{\tau}{\pi^2} H_{0xx} - \frac{\beta}{\pi^4} H_{0xxxx} + \frac{\pi F_v^c}{2} P_{0x} = 0, \\ H_0 = H_{0xx} = 0 \text{ at } x = 0, 1 \quad \text{and} \quad P_0 = 0 \text{ at } x = 1. \end{aligned} \right\} \quad (3.13)$$

To study the evolution of perturbations about this steady state, we substitute

$$h(x, t) = H_0(x) + e^{i\omega t} H_1(x), \quad p(x, t) = P_0(x) + e^{i\omega t} P_1(x) \quad (3.14)$$

in equations (3.3) and (3.8) and linearize the resulting equations for small  $H_1$  and  $P_1$ . We thus get a differential eigenvalue problem for  $H_1$ ,  $P_1$  and  $\omega$  as

$$\left. \begin{aligned} \epsilon \omega H_1 = (H_0^3 P_{1x})_x + 3(H_0^2 H_1 P_{0x})_x, \\ (\omega^2 - 1)H_1 + \frac{\tau}{\pi^2} H_{1xx} - \frac{\beta}{\pi^4} H_{1xxxx} + \frac{\pi F_v^c}{2} P_1 = 0 \end{aligned} \right\} \quad (3.15)$$

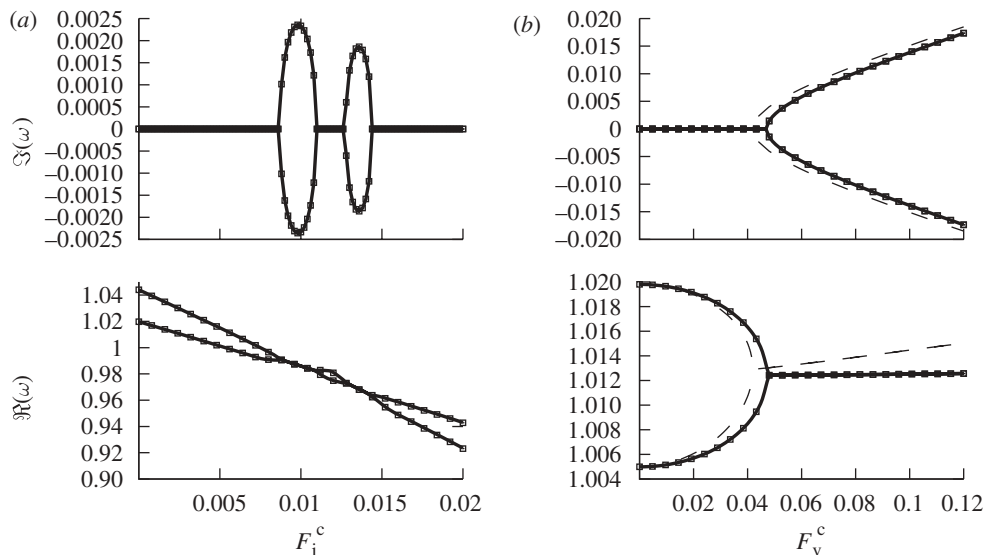


Figure 3. The real and imaginary part of the natural frequency of oscillations for confined flows internal to the elastic structure (see schematic in figure 1). A negative imaginary part implies growth of oscillatory perturbation leading to spontaneously generated flutter. (a) The spectrum for (a) the inviscid case following equation (3.19) and (b) the viscous case following equation (3.11). The parameters used are  $\tau = 0.01$ ,  $\beta = 0$ ,  $\epsilon = 0$  (solid line) and  $\epsilon = 10^{-4}$  (squares). In (b), we also shows the spectrum resulting from a linear stability analysis of (3.3) and (3.8) without any further approximations for  $\epsilon = 10^{-4}$  (dashed line).

with  $H_1 = H_{1xx} = P_1 = 0$  at  $x = 0, 1$ . The functions  $H_0$ ,  $P_0$ ,  $H_1$  and  $P_1$  and the frequency  $\omega$  are determined numerically using a shooting method. The results are compared in figure 3b and agree well with the results of the two-mode truncation (3.12).

### (b) Inviscid flow

If the Reynolds number of the flow is based on the channel width  $Uh/\nu \gg 1$ , we may again revert to the potential flow approximation for fluid flow. In this case, in the absence of analytic approximations we had to resort to numerical solutions for part of our analysis. To simulate the entrance and exit boundary conditions in the neighbourhood of the confined compliant section of interest, we assume that the channel diverges at an angle of  $45^\circ$  upstream and downstream, over a distance of 10 channel widths widening to 10 times the channel height as shown in figure 1. The steady-flow ( $\mathbf{U}$ ) profile is given by the solution of

$$\left. \begin{aligned} \mathbf{U} = \nabla\Phi \quad \text{and} \quad \nabla^2\Phi = 0, \\ \mathbf{U} = U\hat{\mathbf{x}} \text{ as } x \rightarrow \pm\infty \quad \text{and} \quad \mathbf{U} \cdot \mathbf{n} = 0 \text{ on the wall,} \end{aligned} \right\} \quad (3.16)$$

where  $\mathbf{n}$  is the unit outward normal to the wall. The steady pressure on the wall is then given in terms of the Bernoulli equation  $P = -\rho|\mathbf{U}|^2/2$ ; however, we assume that this deflection is negligible in consonance with assumption (i), since the fluid forcing is assumed to be small relative to the elastic forces. When the compliant

section starts to flutter, the perturbed flow potential is given by the solution of the boundary value problem

$$\mathbf{u} = \nabla\phi \quad \text{and} \quad \nabla^2\phi = 0, \quad (3.17)$$

and

$$\phi = 0 \text{ as } x \rightarrow \pm\infty \quad \text{and} \quad h_t + \Phi_x h_x = \phi_y \text{ on the wall} \quad (3.18)$$

and the perturbed hydrodynamic pressure is then given by  $p + \rho(\phi_t + \Phi_x\phi_x + \Phi_y\phi_y) = 0$ . This pressure then couples the mode amplitudes via its projection on the mode shapes given by equation (3.6). We employ the finite element method using the software FreeFem++ by Pironneau *et al.* (2009) for  $\Phi$  and  $\phi$  and thence determine the pressure-induced mode coupling. Using an analysis similar to that performed in §2*a* reveals the dimensionless flow parameter to be  $F_i^c = 2\rho U^2/KH$  (subscript i for inviscid flow and superscript c for confinement).

We now consider the three assumptions outlined in the introduction. Assumption (i) requires that the hydrodynamic pressure is small compared with the elastic forces, i.e.  $P \ll KH$ . As a result, the equilibrium shape of the membrane to leading order is  $h = 1 + O(P/KH)$  and the dominant dynamics are oscillations of each mode with its natural frequency  $\Omega_n^2 = 1 + \tau n^2 + \beta n^4$ . Assumption (ii) requires that the modes are clustered together. If  $\tau = \beta = 0$ , the system is infinitely degenerate with unit frequency, but when  $\tau, \beta \ll 1$  the non-dimensional frequencies of the first few modes are close to unity. Finally, assumption (iii) that the hydrodynamic time scale be smaller than the elastic time scale implies  $\epsilon \ll 1$ . In this case, we truncate our modal expansion after four terms since the odd (even) modes are strongly coupled to only the odd (even) modes. The resulting four-mode truncation of the motion of the compliant boundary given by equation (3.5) leads to the matrix equation

$$\begin{aligned} & \frac{d^2}{dt^2} \begin{bmatrix} A_1 \\ A_2 \\ A_3 \\ A_4 \end{bmatrix} + \sigma \frac{d}{dt} \begin{bmatrix} A_1 \\ A_2 \\ A_3 \\ A_4 \end{bmatrix} \\ &= - \begin{bmatrix} 1 & 0 & 0 & 0 \\ 0 & 1 & 0 & 0 \\ 0 & 0 & 1 & 0 \\ 0 & 0 & 0 & 1 \end{bmatrix} \begin{bmatrix} A_1 \\ A_2 \\ A_3 \\ A_4 \end{bmatrix} - \tau \begin{bmatrix} 1 & 0 & 0 & 0 \\ 0 & 4 & 0 & 0 \\ 0 & 0 & 9 & 0 \\ 0 & 0 & 0 & 16 \end{bmatrix} \begin{bmatrix} A_1 \\ A_2 \\ A_3 \\ A_4 \end{bmatrix} - \beta \begin{bmatrix} 1 & 0 & 0 & 0 \\ 0 & 16 & 0 & 0 \\ 0 & 0 & 81 & 0 \\ 0 & 0 & 0 & 256 \end{bmatrix} \\ & \times \begin{bmatrix} A_1 \\ A_2 \\ A_3 \\ A_4 \end{bmatrix} + F_i^c \begin{bmatrix} 3.6534 & 2.9 \times 10^{-4} & -0.25787 & 3.9 \times 10^{-4} \\ -0.50103 & 7.5060 & -0.23247 & -0.0765 \\ 0.88307 & 3.3 \times 10^{-5} & 11.9040 & 1.4 \times 10^{-6} \\ -0.62126 & 0.92497 & -0.28904 & 16.378 \end{bmatrix} \begin{bmatrix} A_1 \\ A_2 \\ A_3 \\ A_4 \end{bmatrix} \\ & + \epsilon F_i^c \begin{bmatrix} 0.09397 & -1.86224 & -0.03797 & -0.79303 \\ -1.44584 & 0.10882 & -2.38681 & 0.05625 \\ 0.28813 & 1.04022 & 0.07224 & -1.63587 \\ -3.12191 & 0.13495 & 0.11886 & 0.06977 \end{bmatrix} \begin{bmatrix} A_{1t} \\ A_{2t} \\ A_{3t} \\ A_{4t} \end{bmatrix}, \quad (3.19) \end{aligned}$$

where the matrices proportional to  $F_i^c$  and  $\epsilon F_i^c$  are computed numerically. The normal mode frequencies resulting from the analysis of the characteristic equation (3.19) are shown in figure 3*a*. Once again for  $\epsilon = \sigma = 0$ , we see that

when the  $F_1^c > F^*$ , i.e. when the fluid velocity crosses a critical threshold, the real frequencies split into complex conjugate pairs with the consequence that the modal amplitudes grow exponentially, leading to a linear instability. We see two such windows of instability in figure 3*a*, one corresponding to the interaction of modes 1 and 3, and the other corresponding to the interaction of modes 2 and 4. The figure also shows that the cases  $\epsilon \ll 1$  and  $\sigma \ll 1$  closely resemble the  $\epsilon = \sigma = 0$  case.

#### 4. Discussion

We have presented a unified mechanism for the onset of spontaneous oscillations for a class of systems where slender elastic structures are loaded by fluid flow. In particular, by using four extreme cases of geometry and fluid loading on slender elastic structures, corresponding to the cases of viscous and inviscid flows in confined and unconfined geometries, we have demonstrated how the central concept of 1:1 resonance borrowed from dynamical system theory arises naturally. In each case, the natural modes of the elastic structure in free space serve as the oscillators and asymmetrical coupling brought about by the fluid loading leads to a coincidence of frequencies and thence, to an oscillatory instability. These cases are representative of a larger family of problems where all the basic ingredients for 1:1 resonance exist, including the onset of flutter of a flag (a clamped-free elastic beam subject to an external flow), consistent with the results of Argentina & Mahadevan (2005) and recently corroborated by Alben (2008); indeed the essential components of the mechanism are most clearly seen in our analysis of the flat plate in §2*a*.

We find that the critical hydrodynamic forcing for the onset of the instability is proportional to the difference in the natural frequency of free oscillations of the elastic structure. While this is well known to aeronautical engineers, who have known this mechanism of unconfined flutter at least since Rocard (1957) and Pines (1958) (see also Dowell 2004 for a review), here we have extended that conclusion to other systems as well. Similarly, while instabilities in purely viscous flows interacting with compliant walls have been reported before, e.g. Kumaran & Muralikrishnan (2000) and Eggert & Kumar (2004), our generic mechanism provides a unified view of these instabilities for purely viscous flows interacting with soft but massive boundaries.

Since oscillatory instabilities also arise in high Reynolds number flows through collapsible channels and tubes, it is useful to clarify and distinguish the different mechanisms that can lead to these instabilities. To do this, we turn to the classical work of Benjamin (1960) and Landahl (1962) that set the stage for a three-fold classification of instabilities in fluid–structure interaction. Originally intended to apply for boundary layer flows, class A instabilities correspond to the case when the instability is weakly modified by a compliant structure, class B instabilities correspond to the case when elastic modes are weakly modified by fluid flow while class C instabilities are similar to the Kelvin–Helmholtz instability with a signature of a coincidence of frequencies.

Asymptotic and numerical analyses for flutter in other systems such as confined shear flows (see Luo & Pedley 1998; Huang 1998; Huang 2001; Jensen & Heil 2003) have demonstrated that while fluid inertia is the dominant destabilizing effect, viscous effects in the Stokes boundary layer play a stabilizing role in these

systems. Thus in the context of the Benjamin–Landahl scheme, these systems fall into class B where elastic modes are weakly modified by fluid flows. In contrast, by allowing for mode coupling and thus providing a mechanism for frequency coincidence, we have generalized and extended the case of class C instabilities to a broader class of fluid–structure interactions. While the extension of classes A and B instabilities to viscous and inviscid flows beyond boundary layer flows remains an open question, when  $\epsilon \gg 1$ , i.e. when the fluid time scale is slow relative to the time for elastic oscillations suggests how class A instabilities also might arise in a broader class of flows.

We conclude by emphasizing that we have restricted ourselves to a region of the parameter space limited by our three assumptions and it is of interest to examine the consequences when these assumptions are relaxed. In particular, our analysis suggests that by letting the elastic forces also be as weak as the fluid forces, it is possible to excite static deformations of the structure known as ‘divergence’. In the presence of nonlinearities or other effects, this static deformation may acquire a slow time dependence. This may be a possible explanation for volcanic tremor, where the observed time scale is too slow to be explained by normal mode oscillations (Rust *et al.* 2007). Clearly there are many avenues to pursue at this interface between elasticity and hydrodynamics.

We thank Michael Weidman for his contributions to the early work that preceded this study.

## References

- Alben, S. 2008 The flapping-flag instability as a nonlinear eigenvalue problem. *Phys. Fluids* **20**, 104106. (doi:10.1063/1.3000670)
- Argentina, M. & Mahadevan, L. 2005 Fluid-flow-induced flutter of a flag. *Proc. Natl Acad. Sci. USA* **102**, 1829–1834. (doi:10.1073/pnas.0408383102)
- Balmforth, N. J., Craster, R. V. & Rust, A. C. 2005 Instability in flow through elastic conduits and volcanic tremor. *J. Fluid Mech.* **527**, 353–377. (doi:10.1017/S0022112004002800)
- Batchelor, G. K. 1967 *An introduction to fluid mechanics*. Cambridge, UK: Cambridge University Press.
- Benjamin, T. B. 1960 Effects of flexible boundary on hydrodynamic stability. *J. Fluid Mech.* **9**, 513–532. (doi:10.1017/S0022112060001286)
- Bertram, C. D. & Pedley, T. J. 1982 A mathematical model of unsteady collapsible tube behaviour. *J. Biomech.* **15**, 39–50. (doi:10.1016/0021-9290(82)90033-1)
- Billah, K. Y. & Scanlan, R. H. 1991 Resonance, Tacoma Narrows bridge failure, and undergraduate physics textbooks. *Am. J. Phys.* **59**, 118–124. (doi:10.1119/1.16590)
- Bisplinghoff, R. L. & Ashley, H. 1962 *Principles of aeroelasticity*. Mineola, NY: Dover.
- Bisplinghoff, R. L., Ashley, H. & Halfman, R. L. 1955 *Aeroelasticity*. Cambridge, MA: Addison-Wesley.
- Chang, Y. B. & Moretti, P. M. 2002 Flow-induced vibration of free edges of thin films. *J. Fluid Struct.* **16**, 989–1008. (doi:10.1006/jfls.2002.0456)
- Chouet, B. 1985 Excitation of a buried magma pipe: a seismic source model for volcanic tremor. *J. Geophys. Res.* **90**, 1881–1893. (doi:10.1029/JB090iB02p01881)
- Dowell, E. H. (ed.) 2004 *A modern course in aeroelasticity*. Dordrecht, The Netherlands: Kluwer Academic.
- Eggert, M. D. & Kumar, S. 2004 Observations of instability, hysteresis, and oscillation in low-Reynolds-number flow past polymer gels. *J. Colloid Int. Sci.* **278**, 234–242. (doi:10.1016/j.jcis.2004.05.043)
- Fletcher, N. H. 1993 Autonomous vibration of simple pressure-controlled valves in gas flows. *J. Acoust. Soc. Am.* **93**, 2172–2180. (doi:10.1121/1.406857)
- Fung, Y.-C. 2002 *An introduction to the theory of aeroelasticity*. Mineola, NY: Dover Publications.

- Grotberg, J. B. & Jensen, O. E. 2004 Biofluid mechanics in flexible tubes. *Annu. Rev. Flu. Mech.* **36**, 121–147. (doi:10.1146/annurev.fluid.36.050802.12198)
- Happel, J. & Brenner, H. 1983 *Low Reynolds number hydrodynamics: with special applications to particulate media*. Dordrecht, The Netherlands: Kluwer Academic (Print on demand).
- Huang, L. 1998 Reversal of Bernoulli effect and channel flutter. *J. Fluids Struct.* **12**, 131–151. (doi:10.1006/jfls.1997.0131)
- Huang, L. 2001 Viscous flutter of a finite elastic membrane in Poiseuille flow. *J. Fluids Struct.* **15**, 1061–1088. (doi:10.1006/jfls.2001.0392)
- Jensen, O. E. & Heil, M. 2003 High-frequency self-excited oscillations in a collapsible-channel flow. *J. Fluid Mech.* **481**, 235–268. (doi:10.1017/S002211200300394x)
- Julian, B. R. 1994 Volcanic tremor: nonlinear excitation by fluid flow. *J. Geophys. Res.* **99**, 11 859–11 877. (doi:10.1029/93JB03129)
- Kelvin, W. T. & Tait, P. G. 1912 *Treatise on natural philosophy*. Cambridge, UK: Cambridge University Press.
- Korotkoff, N. S. 1905 On the subject of methods of determining blood pressure. *Bull. Imperial Mil. Med. Acad* **11**, 356–367.
- Kumaran, V. & Muralikrishnan, R. 2000 Spontaneous growth of fluctuations in the viscous flow of flow past a soft interface. *Phys. Rev. Lett.* **84**, 3310–3313. (doi:10.1103/physrevlett.84.3310)
- Landahl, M. 1962 On the stability of a laminar incompressible boundary layer over a flexible surface. *J. Fluid Mech.* **13**, 607–632. (doi:10.1017/S002211206200097X)
- Lemaitre, C. & de Langre Hémon, E. P. 2007 Thin water film around a cable subject to wind. *J. Wind Eng.* **95**, 1259–1271. (doi:10.1016/j.jweia.2007.02.007)
- Luo, X.-Y. & Pedley, T. J. 1998 The effects of wall inertia on flow in a two-dimensional collapsible channel. *J. Fluid Mech.* **363**, 253–280. (doi:10.1017/S0022112098001062)
- Miyata, T. 2003 Historical view of long-span bridge aerodynamics. *J. Wind Eng. Ind. Aerodyn.* **91**, 1393–1410. (doi:10.2471/BLT.06.037671)
- Müller, C., Schlindwein, V., Eckstaller, A. & Miller, H. 2005 Singing icebergs. *Science* **310**, 1299–1299. (doi:10.1126/science.1117145)
- Paidoussis, M. P. 1998 *Fluid–structure interactions: slender structures and axial flow*. San Diego, CA: Academic Press.
- Pedley, T. J. 1990 *Fluid mechanics of large blood vessels*. Cambridge, UK: Cambridge University Press.
- Pines, S. 1958 An elementary explanation of the flutter mechanism. In *Proc. National Specialists Meeting on Dynamics and Aeroelasticity*, pp. 52–58. New York, NY: Institute of Aeronautical Sciences.
- Pironneau, O., Hecht, F. & Morice, J. 2009 Freefem++. See <http://www.freefem.org/ff++>.
- Rocard, Y. 1957 *Dynamic instability: automobiles, aircraft, suspension bridges*. New York, NY: F. Ungar Publication.
- Rust, A. C., Mandre, S. & Balmforth, N. J. 2007 The feasibility of generating low-frequency volcano seismicity by flow through a deformable channel. *Geological Society of London Special Publications*, **307**, pp. 45–56. London, UK: Geological Society of London.
- Tarnopolsky, A. Z., Fletcher, N. H. & Lai, J. C. S. 2000 Oscillating reed valves — an experimental study. *J. Acoust. Soc. Am.* **108**, 400–406. (doi:10.1121/1.429473)
- Theodorsen, T. 1935 General theory of aerodynamic instability and the mechanism of flutter. Technical Report no. 496. National Advisory Committee for Aeronautics (NACA). Also available online at <http://ntrs.nasa.gov>.
- Titze, I. R. 1988 The physics of small-amplitude oscillation of the vocal folds. *J. Acoust. Soc. Am.* **83**, 1536–1552. (doi:10.1121/1.395910)
- Watanabe, Y., Isogai, K., Suzuki, S. & Sugihara, M. 2002a A theoretical study of paper flutter. *J. Fluid Struct.* **16**, 543–560. (doi:10.1006/jfls.2001.0436)
- Watanabe, Y., Suzuki, S., Sugihara, M. & Sueoka, Y. 2002b An experimental study of paper flutter. *J. Fluid Struct.* **16**, 529–542. (doi:10.1006/jfls.2001.0435)
- Zhang, J., Childress, S., Libchaber, A. & Shelley, M. 2000 Flexible filaments in a flowing soap film as a model for one-dimensional flags in a two-dimensional wind. *Nature* **408**, 835–839. (doi:10.1038/35048530)